9.3 THE SENSITIVITY OF A SIMULATED SUPERCELL TO EMULATED RADIATIVE COOLING BENEATH THE ANVIL

Paul Markowski* and Jerry Harrington

Department of Meteorology, Pennsylvania State University, University Park, PA

1. Motivation

a. Long-lived convective storms and radiative transfer processes

Even though numerical simulations often have produced convective storms that closely resemble those that have been observed, a potentially important forcing frequently has been ignored in these simulations—the influence of radiative effects on storm dynamics. It is true that some two-dimensional numerical studies of mesoscale convective systems previously have included longwave radiative transfer processes. For example, it has been shown that the formation of the well-documented transition zone in MCSs (Smull and Houze 1985; Rutledge and Houze 1987; Biggerstaff and Houze 1993) can be sensitive to longwave radiation (Chen and Cotton 1988; Chin 1994; Braun et al. 1996). Furthermore, longwave radiation effects are known to affect the circulation within the trailing stratiform regions of simulated MCSs (Chen and Cotton 1988; Dudhia 1989; Churchill and Houze 1991; Tao et al. 1991), ultimately enhancing precipitation amounts within the stratiform regions (Tao et al. 1993), which typically account for a significant fraction (up to 50%) of the total precipitation produced by MCSs (Houze 1977; Zipser et al. 1981; Gamanche and Houze 1983; Rutledge and Houze 1987; Johnson and Hamilton 1988).

Although the studies cited above have made important contributions toward our understanding of MCSs, the full range of possible dynamical effects owing to radiative effects, especially those owing to shortwave radiative transfer processes, remains uncertain due to the model dimensionality of these previous studies. In three-dimensional numerical simulations of MCSs (e.g., Rotunno et al. 1988; Weisman et al. 1988; Dudhia and Moncrieff 1989; Weisman 1992, 1993; Skamarock et al. 1994; Trier et al. 1997, 1998), radiative effects generally have not been considered, although Tucker and Crook (1999) recently simulated an MCS case with and without solar radiation. They found that the inclusion of solar radiative effects reduced the intensity of the MCS, although the details of how solar radiative effects were included were not presented.

Radiative effects also have virtually always been excluded from three-dimensional simulations of supercell storms, even though computing power has increased exponentially since the seminal studies of the late 1970s and early 1980s (e.g., Schlesinger 1975; Klemp and Wilhelmson 1978a,b; Wilhelmson and Klemp 1978; Rotunno and Klemp 1982; Klemp and Rotunno 1983). Some recent three-dimensional case study simulations of supercellular convection have included radiation, but these parameterizations have been rather crude. For example, often clouds were seen only as areas of very high water vapor content, with the radiative characteristics of condensed liquid and ice species not taken into account (e.g., Finley et al. 2001), leading to overestimates of solar fluxes reaching the surface in cloudy regions and underestimates of longwave cooling at cloud tops. Furthermore, to our knowledge, in the two- and three-dimensional simulations (of both MCSs and supercells) that *have* included radiation, no sensitivity analyses were done to quantify the effects of radiation on storm dynamics. The exclusion of radiative effects in the majority of convective storm simulation studies (particularly three-dimensional simulations) has been justified with the assumption that radiative processes are unimportant on the time scales of the model integration (e.g., Trier et al. 1997, 1998), and that the storms are "largely dynamically (not radiatively) driven" (Finley et al. 2001). Of course, all of the above statements are true in some sense, for the past apparent modeling successes likely would not have been achieved otherwise. However, what we argue here, and what we currently are examining, is the possibility that convective storms may be *modulated* in certain, and perhaps significant, ways by radiative effects.

b. Observations of significant radiative effects attributable to long-lived convective storms

It is well known that low-level baroclinity can have an important influence on convective storm dynamics. For example, low-level baroclinic zones (gust fronts) commonly are associated with the precipitation regions of convective storms. Klemp and Rotunno (1983) and Rotunno and Klemp (1985) showed that the forward-flank gust front of supercell thunderstorms (Lemon and Doswell 1979) may be an important source of horizontal vorticity for the updrafts of the storms. This horizontal vorticity is generated solenoidally along the boundary separating rain-cooled outflow from the relatively warm inflow. Large vertical velocity gradients associated with the updraft may tilt this horizontal vorticity to give rise to significant low-level vertical vorticity in supercell storms. It also has been shown that baroclinic boundaries associated with the precipitation regions of *other* storms (e.g., adjacent storms or even storms occurring earlier in the day)

* *Corresponding author address*: Dr. Paul Markowski, Department of Meteorology, Pennsylvania State University, 503 Walker Building, University Park, PA 16802; *e-mail*: pmarkowski@psu.edu.

may have similarly important dynamical consequences. For example, when a storm crosses the outflow boundary left behind by some other region of convection, the storm may ingest enhanced baroclinic horizontal vorticity residing along the outflow boundary, which may lead to rapid intensification of low-level rotation (and often tornadogenesis), following tilting and stretching of the augmented horizontal vorticity (Purdom 1976; Maddox et al. 1980; Weaver and Nelson 1982; Markowski et al. 1998a; Atkins et al. 1999; Rasmussen et al. 2000). Even subtle low-level static stability changes not associated with horizontal gradients are known to have significant impacts on storm behavior, and possibly even tornadogenesis (McCaul and Weisman 2001; Markowski et al. 2003a).

Although the potential dynamical importance of low-level baroclinic zones associated with the precipitation regions of convection is well-established, the dynamical significance of low-level baroclinic zones arising from radiative effects associated with convective storms previously have not been examined. Yet the magnitude of the low-level temperature perturbations and baroclinity due to anvil-generated radiative effects has been found to be comparable to the magnitude of baroclinity associated with storm-scale precipitation regions in at least some cases. This may not be entirely surprising. Even in stratiform precipitation events (e.g., those associated with cold-air damming), radiative effects have been found, at least in a few cases, to exert a greater influence on the low-level stability and horizontal temperature gradients than latent cooling associated with the evaporation of precipitation (e.g., Fritsch et al. 1982).

Markowski et al. (1998b) showed that baroclinic zones arising from surface cooling beneath optically thick anvils may be capable of generating horizontal vorticity of the same order of magnitude as that which is often generated along the more extensively studied gust fronts, and also of the same magnitude as the horizontal vorticity associated with the mean vertical wind shear of the ambient, large-scale environment [O(10^{-2}) s^{-1}]. Such horizontal vorticity can be converted to vertical vorticity within storm updrafts via tilting, then amplified by stretching (Rotunno 1981; Davies-Jones 1984; Klemp 1987). Deep, persistent updraft rotation is the defining characteristic of supercell storms; thus, means of enhancing low-level horizontal vorticity may have important implications for the dynamics of such storms, in addition to the dynamics of other types of convective storms.

In the cases documented by Markowski et al. (1998b), temperature deficits as large as 5–6 K were found to develop within the anvil shadows. The temperature differences were observed to occur over horizontal distances of ∼25 km. The rate at which horizontal vorticity is generated by such a baroclinic zone exceeds 0.02 s^{-1} h^{-1}. The temperature gradients and associated vorticity generation rates owing to the anvil shadows may be smaller than temperature gradients often associated with the gust fronts of convective storms (∼5 K km^{-1}). However, parcel residence times within anvil-generated baroclinic zones (Markowski et al. estimated the time scales to be ∼1 h) would generally be larger than parcel residence times within the baroclinic zones associated with storm-scale gust fronts (∼5–15 min), due to the larger horizontal scale of the anvil shadow compared to the scale of the precipitation region of the storm. Thus, the total horizontal vorticity generated baroclinically may be comparable to that produced by low-level outflow [O(10^{-2}) s^{-1}].

One question that Markowski et al. (1998b) were unable to fully address was the depth over which the cooling and baroclinity developed. A few soundings indicated that the low-level baroclinity was likely several hundred meters in depth. Although it is not known how deep the baroclinity must extend for significant dynamical effects to arise, there is growing evidence that modifications of just the lowest few hundred meters of the environmental vertical wind profile may have profound effects on storm behavior (Wicker 1996; Markowski et al. 2003b). Low-level temperature modifications by anvils also affect the convective available potential energy (CAPE) and convective inhibition (CIN) of the storm environment. It is not known what effects these alterations may have on convective storm behavior when included in a numerical simulation. Furthermore, it is not known how the effects of baroclinic vorticity differ depending on whether the baroclinic vorticity has been generated within a region in which equivalent potential temperature (θ_e) has been nearly conserved (as might be expected to be the case along gust fronts where cooling is largely due to evaporation of precipitation), or whether the baroclinic vorticity has been generated within a region in which θ_e deficits also have been generated (as might be expected to be the case where cooling owes to radiative effects). Even the forward speed of the convective storm might reasonably be expected to affect the magnitude of the radiative effects, at least those related to surface cooling due to a reduction of incident shortwave radiation. For example, a rapidly moving storm with its attendant anvil will constantly be encountering warm ground that it will have to cool in order to develop surface temperature gradients. On the other hand, a stationary storm can shade the same ground for a longer period of time, thereby producing correspondingly larger surface temperature gradients. Conversely, the development of surface temperature gradients in storms due to low-level evaporative cooling is Galilean invariant, since the precipitation region (which produces the cooling) moves with the storm.

2. Numerical simulations with emulated radiative cooling

We have completed a pair of preliminary simulations in order to illustrate the potentially important effects of radiative transfer processes on convective storm dynamics. The relatively coarse-resolution demonstration simulations were conducted using version 4.5.2 of the Advanced Regional Prediction System (ARPS; Xue et al. 2000, 2001). The simulations were initialized with the composited sounding from the well-documented 20 May 1977 Del City, Oklahoma, storm (Ray et al. 1981; Johnson et al. 1987), which has been used in several other modeling studies (e.g., Klemp et al. 1981; Klemp and Rotunno 1983; Grasso and Cotton 1995; Adlerman et al. 1999; Adlerman and Droegemeier 2002). This sounding is char-

acterized by a CAPE of approximately 2600 J kg^{-1} and a 0–3 km storm-relative helicity of approximately 150 m^2 s^{-2} (Fig. 1). The hodograph has been shifted by a mean velocity so that the mature, cyclonically rotating storm is nearly stationary. One of the demonstration simulations (the control) was run without surface physics and radiation. In the other demonstration simulation, radiative cooling due to anvil shading was emulated by prescribing a cooling rate to the skin temperature of 5 K h^{-1} at any grid point at which cloud water was present overhead. This skin cooling rate is similar to that observed by Markowski et al. (1998b). Low-level air temperatures were coupled to the skin cooling in this second simulation by the inclusion of surface sensible heat fluxes using simple bulk aerodynamic drag laws (latent and soil heat fluxes were not included). Though this emulation of radiative cooling is admittedly simple, it should suffice to illustrate the potential effects that radiative cooling under the anvil may have on storm dynamics. The domain was 200×200×18 km. The horizontal resolution was 1000 m, and the vertical resolution varied from 150 m in the boundary layer to 500 m near the tropopause. Only warm-rain (Kessler) microphysics is used for both of the idealized demonstration simulations. Though this microphysical simplification is not necessary for our demonstration, we choose to use warm-rain only for two reasons: computational expedience and, more importantly, neglecting ice processes leads to an anvil of smaller areal extent. Hence, if radiative cooling is important here, its importance will likely be amplified in the presence of a longer, thicker anvil. Neither simulation includes the Coriolis force.

The evolution of both experiments in the first hour is similar and will not be discussed in detail [see Klemp et al. (1981) for a more detailed discussion]. The initial updraft splits into anticyclonically (left-moving) and cyclonically ("right-moving"—note that the hodograph was shifted so that the right-moving storm would be nearly stationary) rotating cells approximately 20 min into the simulations. The cyclonically rotating cell dominates throughout the rest of the simulations, becoming a mature supercell approximately after 40 min have elapsed. By about 60 min, the supercell takes on a nearly steady-state character in both simulations, with a persistent midlevel (3–7 km) mesocyclone and updrafts greater than 30 m s^{-1}.

The purpose of the demonstration simulations is to show that, beyond roughly the first 60 min, there are *significant differences between the two supercells—differences that can only be due to effects associated with the emulated anvil shading.* Our goal is not to present detailed diagnostics of the model output here, elucidating the precise dynamics responsible for the simulation differences, for this is one of the goals of our ongoing research. *Our goal here is only to show that radiative effects associated with cirrus anvils can have a significant impact on convective storm characteristics.*

Figs. 2 and 3 show the cloud water isosurface and low-level wind vectors, isotherms, and rain water fields for the control and emulated anvil shading simulations, respectively. The surface cooling beneath the anvil is readily identifiable in Fig. 3 (cf. Fig. 2). Although the temperature deficits beneath the anvil might be considered to be small (only 1–3 K) and shallow (see Fig. 1), the expansive region of surface cooling in the storm inflow had an effect on subsequent storm morphology that can be regarded as substantial. For example, the time series of vertical velocity and vertical vorticity (Fig. 4) have large differences, with the maximum vertical velocity (low-level vertical vorticity) values observed during the simulations differing by 20% (100%) at times.

The supercell simulated without radiative effects generally has much stronger low-level rotation compared to the supercell simulated with the emulated anvil shading effect (Fig. 4). The near-surface vector wind fields are quite different at $t = 2$ h (Figs. 2 and 3), with the stronger rotation clearly evident in the control simulation. In fact, the differences in the near-surface vector wind fields in the simulated storms are much larger than those that have been observed between tornadic and nontornadic supercells (Blanchard and Straka 1998; Trapp 1999; Wakimoto and Cai 2000; Markowski et al. 2002). The low-level potential temperature fields, and especially the orientation and magnitude of the gradients, in close proximity to the storms, had readily discernible differences (Figs. 2 and 3); thus, it is not surprising that large kinematic differences (e.g., the vertical vorticity differences) would result, given the well-known relationship between temperature gradients, horizontal vorticity modulation, and vertical vorticity generation by tilting.

We reiterate that a detailed investigation of the causes of these differences is beyond what we can do for demonstration purposes, but that the results displayed in Figs. 2, 3, and 4 quite clearly indicate that substantial modifications of storm behavior can be brought about by radiative processes. In this pair of example simulations, it appears as though low-level cooling beneath the anvil has had a detrimental effect on the convective storm. In other cases, e.g., cases in which the orientation of the low-level inflow with respect to the low-level baroclinity is more favorable, it is quite possible that anvils could have an enhancing effect on a convective storm.

A few additional comments are in order concerning the demonstration simulations. The long-lived supercell storms simulated in the pair of demonstration simulations were nearly stationary. Thus, it might seem that the simulation with emulated radiative cooling perhaps exaggerated the effect of anvil shading, due to shading of the same region for a long duration. However, the surface temperature deficit and associated horizontal baroclinity beneath the anvil, even after 3 hours (not shown), were not as large as has been observed. Furthermore, the hodograph structure (Fig. 1) was not ideal—not only did low-level inflow parcels fail to spend much time in the anvil-generated baroclinic zone, but the baroclinic zone itself was situated so that inflow entering the updraft did not pass through the (southern) portion of the baroclinic zone that would have augmented the horizontal vorticity associated with the base state vertical wind shear. Instead, the horizontal vorticity produced by the anvil-generated baroclinic zone actually *opposed* the horizontal vorticity associated with the base state vertical wind shear. Perhaps this is

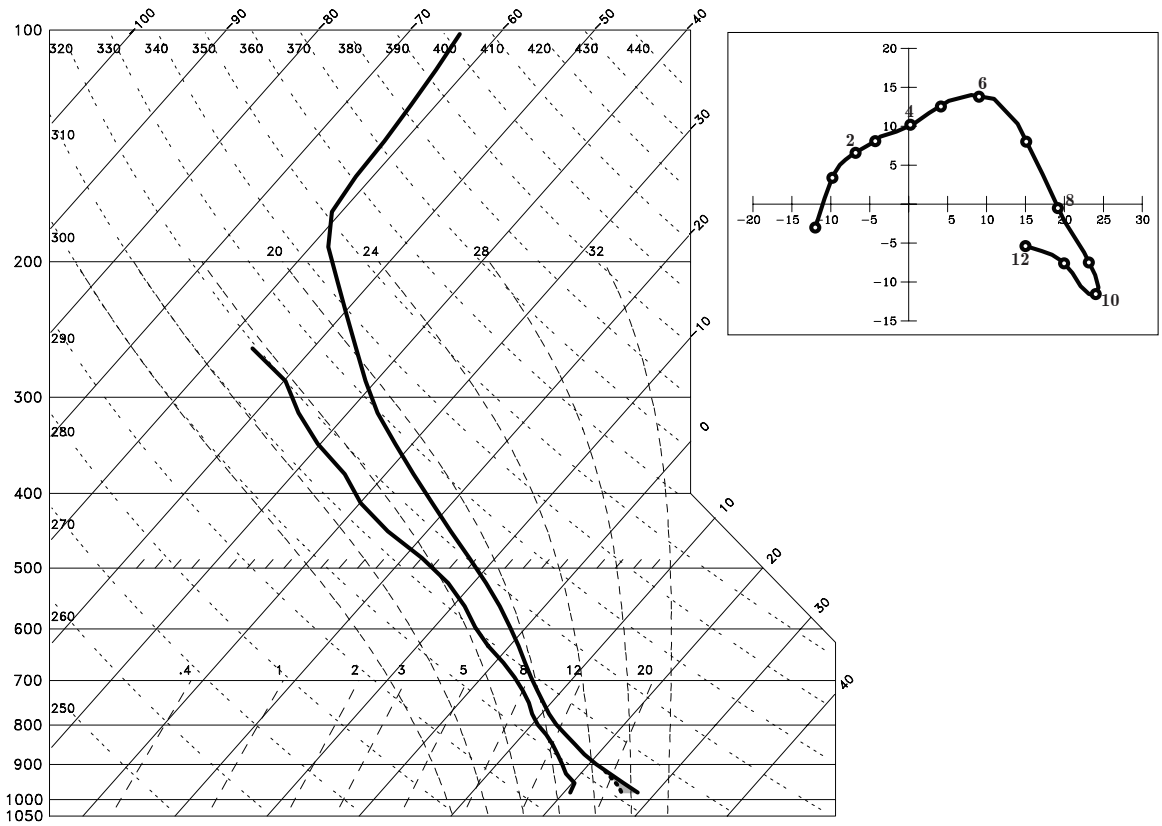

FIG. 1. Skew T-log p diagram (left) and hodograph (right) used to initialize the demonstration simulations. The dashed low-level temperature profile on the sounding indicates the temperature profile at location A in Fig. 3 (within the anvil shadow). Units on the hodograph are m s^{-1}, and open circles (every other one is labeled in km) are placed along the hodograph at 1 km intervals.

why the storm associated with low-level anvil baroclinity had weaker near-surface rotation. Or, perhaps there are other reasons that will be discovered upon completing future diagnostics, such as increased CIN in the inflow. It is also worth noting that the demonstration simulations did not include ice physics. The inclusion of ice physics leads to the production of more expansive anvils (and therefore *more expansive* surface temperature modifications) compared to the warm-rain microphysical parameterization used for the demonstration simulations (Gilmore and Wicker 1998). Given the above-noted departures from what might be considered to be much more ideal conditions for magnifying the importance of anvil radiative effects on convective storms, we believe that the demonstration simulations *quite conservatively* indicate that radiative effects can have a significant effect on convective storms.

It does not seem likely that radiative effects would be important in all convective storms. For example, short-lived storms probably would not be affected by radiatively-cooled shadow regions, owing to their relatively brief duration and small anvils. On the other hand, long-lived storms might be more prone to radiative effects on their dynamics, owing to their larger anvil canopies and longer storm time scales. Furthermore, long-lived storms tend to occur in environments containing large vertical wind shear, which promotes storm organization and longevity. Large vertical wind shear typically is associated with strong storm-relative winds at anvil level, leading to the formation of long anvils in the downstream direction, overlying the storm inflow region, where surface shading effects may have the largest impact. Also, the most dangerous convective storms often are isolated, and thus may have a well-defined anvil shadow edge and associated low-level baroclinity.

3. Work in progress

The preliminary work summarized herein represents the first step of a larger effort to explore the effects of radiative transfer processes on isolated convective storms. Our next step is to include radiative effects and more sophisticated microphysics in a series of simulations designed to establish bounds on the magnitude of radiative effects on long-lived convective storms, as well as the nature of these effects and how these effects depend on storm morphology and the ambient environment.

REFERENCES

Adlerman, E. J., and K. K. Droegemeier, 2002: The sensitivity of numerically simulated cyclic mesocyclogenesis to variations in model physical and computational parameters. *Mon. Wea. Rev.*, **130**, 2671–2691.

Adlerman, E. J., K. K. Droegemeier, and R. Davies-Jones, 1999: A numerical simulation of cyclic mesocyclogenesis. *J. Atmos. Sci.*, **56**, 2045–2069.

Atkins, N. T., M. L. Weisman, and L. J. Wicker, 1999: The inuence of preexisting boundaries on supercell evolution. *Mon. Wea. Rev.*, **127**, 2910–2927.

Biggerstaff, M. I., and R. A. Houze, 1993: Kinematics and microphysics of the transition zone of the 10–11 June 1985 squall line. *J. Atmos. Sci.*, **50**, 3091–3110.

Blanchard, D. O., and J. M. Straka, 1998: Some possible mechanisms for tornadogenesis failure in a supercell. Preprints, *19th Conf. on Severe Local Storms.* Minneapolis, Amer. Meteor. Soc., 116–119.

Braun, S. A., R. A. Houze, and M.-J. Yang, 1996: Comments on "The Impact of the Ice Phase and Radiation on a Midlatitude Squall Line System." *J. Atmos. Sci.*, **53**, 1343–1351.

Chen, S., and W. R. Cotton, 1988: The sensitivity of a simulated extratropical mesoscale convective system to longwave radiation and ice-phase microphysics. *J. Atmos. Sci.*, **45**, 3897–3910.

Chin, H.-N., 1994: The impact of the ice phase and radiation on a midlatitude squall line system. *J. Atmos. Sci.*, **51**, 3320–3343.

Churchill, D. D., and R. A. Houze, 1991: Effects of radiation and turbulence on the diabatic heating and water budget of the stratiform region of a tropical cloud cluster. *J. Atmos. Sci.*, **48**, 903–922.

Davies-Jones, R. P., 1984: Streamwise vorticity: The origin of updraft rotation in supercell storms. *J. Atmos. Sci.*, **41**, 2991–3006.

Dudhia, J., 1989: Numerical study of convection observed during the Winter Monsoon Experiment using a mesoscale two-dimensional model. *J. Atmos. Sci.*, **46**, 3077–3107.

Dudhia, J., and M. W. Moncrieff, 1989: A three-dimensional numerical study of an oklahoma squall line containing right-flank supercells. *J. Atmos. Sci.*, **46**, 3363–3391.

Finley, C. A., W. R. Cotton, and R. A. Pielke, 2001: Numerical simulation of tornadogenesis in a high-precipitation supercell. Part I: Storm evolution and transition into a bow echo. *J. Atmos. Sci.*, **58**, 1597–1629.

Fritsch, J. M., J. Kapolka, and P. A. Hirschberg, 1992: The effects of subcloud-layer diabatic processes on cold air damming. *J. Atmos. Sci.*, **49**, 49–70.

Gilmore, M. S., and L. J. Wicker, 1998: The influence of midtropospheric dryness on supercell morphology and evolution. *Mon. Wea. Rev.*, **126**, 943–958.

Grasso, L. D., and W. R. Cotton, 1995: Numerical simulation of a tornado vortex. *J. Atmos. Sci.*, **52**, 1192–1203.

Houze, R. A., 1977: Structure and dynamics of a tropical squall line system.*Mon. Wea. Rev.*, **105**, 1540–1567.

Johnson, K. W., P. S. Ray, B. C. Johnson, and R. P. Davies-Jones, 1987: Observations related to the rotational dynamics of the 20 May 1977 tornadic storms. *Mon. Wea. Rev.*, **115**, 2463–2478.

Johnson, R. H., and P. J. Hamilton, 1988: The relationship of surface pressure features to the precipitation and airow structure of an intense midlatitude squall line. *Mon. Wea. Rev.*, **116**, 1444–1471.

Klemp, J. B., 1987: Dynamics of tornadic thunderstorms. *Ann. Rev. Fluid Mech.*, **19**, 369–402.

Klemp, J. B., and R. Rotunno, 1983: A study of the tornadic region within a supercell thunderstorm. *J. Atmos. Sci.*, **40**, 359–377.

Klemp, J. B., and R. B. Wilhelmson, 1978a: The simulation of three-dimensional convective storm dynamics. *J. Atmos. Sci.*, **35**, 1070–1096.

Klemp, J. B., and R. B. Wilhelmson, 1978b: Simulations of right- and left-moving storms produced through storm splitting. *J. Atmos. Sci.*, **35**, 1097–1110.

Klemp, J. B., R. B. Wilhelmson, and P. S. Ray, 1981: Observed and numerically simulated structure of a mature supercell thunderstorm. *J. Atmos. Sci.*, **38**, 1558–1580.

Lemon, L. R., and C. A. Doswell, 1979: Severe thunderstorm evolution and mesocyclone structure as related to tornadogenesis. *Mon. Wea. Rev.*, **107**, 1184–1197.

Maddox, R. A., L. R. Hoxit, and C. F. Chappell, 1980: A study of tornadic thunderstorm interactions with thermal boundaries. *Mon. Wea. Rev.*, **108**, 322–336.

Markowski, P. M., E. N. Rasmussen, and J. M. Straka, 1998a: The occurrence of tornadoes in supercells interacting with boundaries during VORTEX-95. *Wea. Forecasting*, **13**, 852–859.

Markowski, P. M., E. N. Rasmussen, J. M. Straka, and D. C. Dowell, 1998b: Observations of low-level baroclinity generated by anvil shadows. *Mon. Wea. Rev.*, **126**, 2942–2958.

Markowski, P. M., E. N. Rasmussen, and J. M. Straka, 2002: Direct surface thermodynamic observations within the rear-flank downdrafts of nontornadic and tornadic supercells. *Mon. Wea. Rev.*, **130**, 1692–1721.

Markowski, P. M., J. M. Straka, and E. N. Rasmussen, 2003a: Tornadogenesis resulting from the transport of circulation by a downdraft: Idealized numerical simulations. *J. Atmos. Sci.*, **60**, 795–823.

Markowski, P. M., C. Hannon, J. Frame, E. Lancaster, A. Pietrycha, R. Edwards, and R. Thompson, 2003b: Characteristics of vertical wind profiles near supercells obtained from the Rapid Update Cycle. *Wea. Forecasting*, **18**, 1262–1272.

McCaul, E. W., and M. L. Weisman, 2001: The sensitivity of simulated supercell structure and intensity to variations in the shapes of environmental buoyancy and shear profiles. *Mon. Wea. Rev.*, **129**, 664–687.

Purdom, J. F. W., 1976: Some uses of high-resolution GOES imagery in the mesoscale forecasting of convection and its behavior. *Mon. Wea. Rev.*, **104**, 1474–1483.

Rasmussen, E. N., S. J. Richardson, J. M. Straka, P. M. Markowski, and D. O. Blanchard, 2000: The association of significant tornadoes with a baroclinic boundary on 2 June 1995. *Mon. Wea. Rev.*, **128**, 174–191.

Rotunno, R., 1981: On the evolution of thunderstorm rotation. *Mon. Wea. Rev.*, **109**, 577–586.

Rotunno, R., and J. B. Klemp, 1982: The influence of the shear-induced pressure gradient on thunderstorm motion. *Mon. Wea. Rev.*, **110**, 136–151.

Rotunno, R., and J. B. Klemp, 1985: On the rotation and propagation of simulated supercell thunderstorms. *J. Atmos. Sci.*, **42**, 271–292.

Rotunno, R., J. B. Klemp, and M. L. Weisman, 1988: A theory for strong, long-lived squall lines. *J. Atmos. Sci.*, **45**, 463–485.

Rutledge, S. A., and R. A. Houze, 1987: A diagnostic modeling study of the trailing stratiform region of a midlatitude squall line. *J. Atmos. Sci.*, **44**, 2640–2656.

Schlesinger, R. E., 1975: A three-dimensional numerical model of an isolated deep convective cloud: Preliminary results. *J. Atmos. Sci.*, **32**, 934–957.

Skamarock, W. C., M. L. Weisman, and J. B. Klemp, 1994: Three-dimensional evolution of simulated long-lived squall lines. *J. Atmos. Sci.*, **51**, 2563–2583.

Smull, B. F., and R. A. Houze, 1985: A midlatitude squall line with a trailing region of stratiform rain: Radar and satellite observations. *Mon. Wea. Rev.*, **113**, 117–133.

Tao, W.-K., J. Simpson, and S.-T. Soong, 1991: Numerical simulation of a subtropical squall line over Taiwan Strait. *Mon. Wea. Rev.*, **119**, 2699–2723.

Tao, W.-K., J. Simpson, C. H. Sui, B. Ferrier, S. Lang, J. Scala, M. D. Chou, and K. Pickering, 1993: Heating, moisture, and water budgets of tropical and midlatitude squall lines: Comparisons and sensitivity to longwave radiation. *J. Atmos. Sci.*, **50**, 673–690.

Trapp, R. J., 1999: Observations of non-tornadic low-level mesocyclones and attendant tornadogenesis failure during VORTEX. *Mon. Wea. Rev.*, **127**, 1693–1705.

Trier, S. B., M. A. LeMone, and W. C. Skamarock, 1998: Effect of three-dimensional structure on the stormwide horizontal accelerations and momentum budget of a simulated squall line. *Mon. Wea. Rev.*, **126**, 2580–2598.

Trier, S. B., W. C. Skamarock, and M. A. LeMone, 1997: Structure and evolution of the 22 February 1993 TOGA COARE squall line: Organization mechanisms inferred from numerical simulation. *J. Atmos. Sci.*, **54**, 386–407.

Tucker, D. F., and N. A. Crook, 1999: The generation of a mesoscale convective system from mountain convection. *Mon. Wea. Rev.*, **127**, 1259–1273.

Wakimoto, R. M., and H. Cai, 2000: Analysis of a nontornadic storm during VORTEX-95. *Mon. Wea. Rev.*, **128**, 565–592.

Weaver, J. F., and S. P. Nelson, 1982: Multiscale aspects of thunderstorm gust fronts and their effects on subsequent storm development. *Mon. Wea. Rev.*, **110**, 707–718.

Weisman, M. L., 1992: The role of convectively generated rear-inflow jets in the evolution of long-lived mesoconvective systems. *J. Atmos. Sci.*, **49**, 1826–1847.

Weisman, M. L., 1993: The genesis of severe, long-lived bow echoes. *J. Atmos. Sci.*, **50**, 645–645.

Weisman, M. L., J. B. Klemp, and R. Rotunno, 1988: The structure and evolution of numerically simulated squall lines. *J. Atmos. Sci.*, **45**, 1990–2013.

Wicker, L. J., 1996: The role of near surface wind shear on low-level mesocyclone generation and tornadoes. Preprints, *18th Conf. on Severe Local Storms.* San Francisco, Amer. Meteor. Soc., 115–119.

Wilhelmson, R. B., and J. B. Klemp, 1978: A numerical study of storm splitting that leads to long-lived storms. *J. Atmos. Sci.*, **35**, 1974–1986.

Xue, M., K. K. Droegemeier, and V. Wong, 2000: The Advanced Regional Prediction System (ARPS): A multiscale nonhydrostatic atmospheric simulation and prediction tool. Part I: Model dynamics and verification. *Meteor. Atmos. Phys.*, **75**, 161–193.

Xue, M., K. K. Droegemeier, V. Wong, A. Shapiro, K. Brewster, F. Carr, D. Weber, Y. Liu, and D. H. Wang, 2001: The Advanced Regional Prediction System (ARPS): A multiscale nonhydrostatic atmospheric simulation and prediction tool. Part II: Model physics and applications. *Meteor. Atmos. Phys.*, **76**, 143–165.

Zipser, E. J., 1977: Mesoscale and convective-scale downdrafts as distinct components of squall line circulation. *Mon. Wea. Rev.*, **105**, 1568–1589.

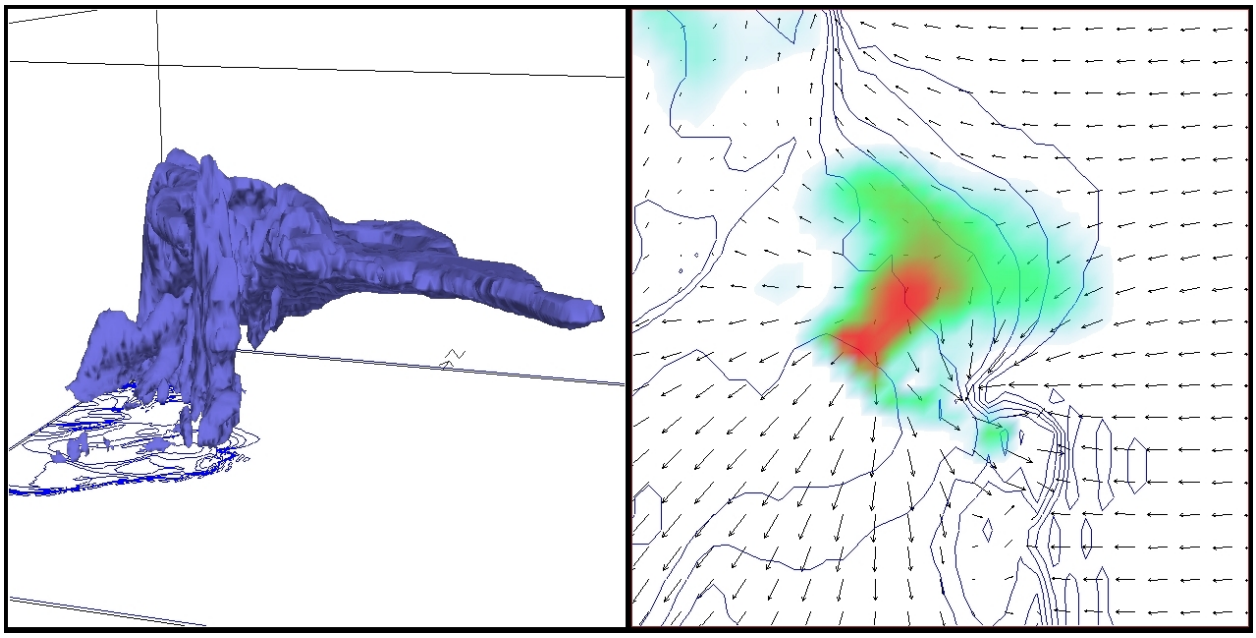

FIG. 2. Simulation results at $t = 2$ h in the simulation in which radiative effects are excluded. (Left) Isosurface depicting the region of cloud water exceeding 0.1 g kg^{-1} and potential temperature deficits at 75 m (1 K contour interval, beginning with $\theta' = -1$ K). (Right) Close-up view of the cyclonic supercell. The rain water field at 1 km is shaded with colors ranging from green to red (green represents light rain and red represents heavy rain), and horizontal wind vectors and the potential temperature deficit field (1 K contour interval, beginning with $\theta' = -1$ K) at 75 m also are displayed.

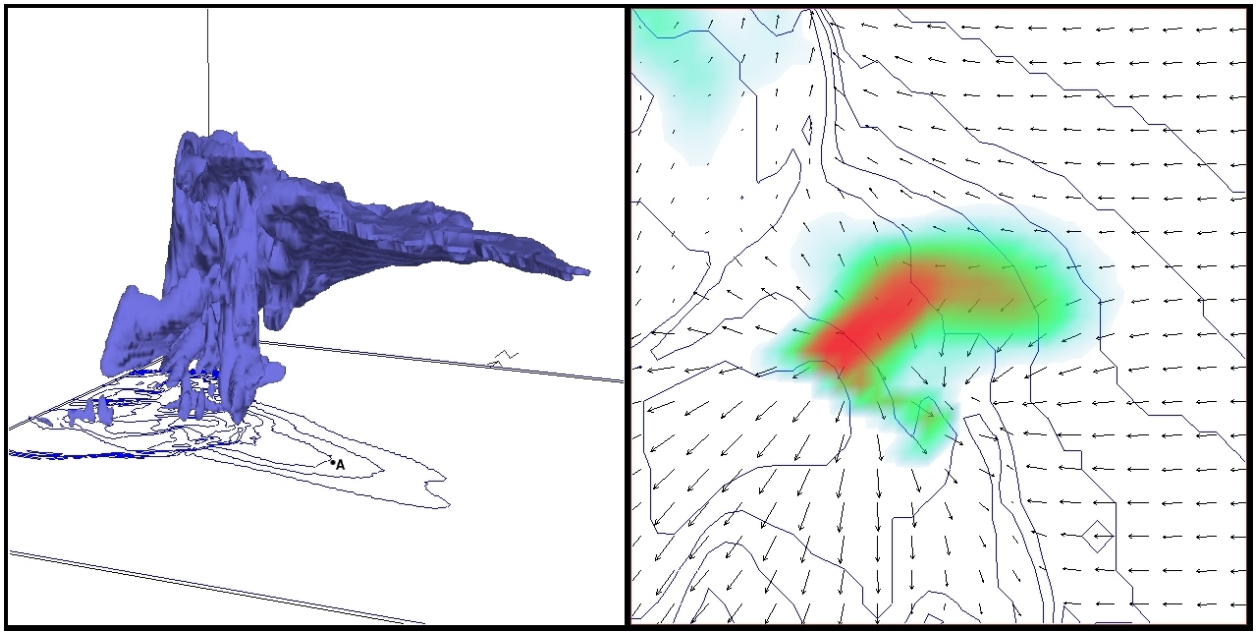

FIG. 3. As in Fig. 2, but for the simulation in which shortwave radiative cooling was emulated beneath the storm anvil. The low-level sounding at location "A" in the left frame is overlaid in Fig. 1.

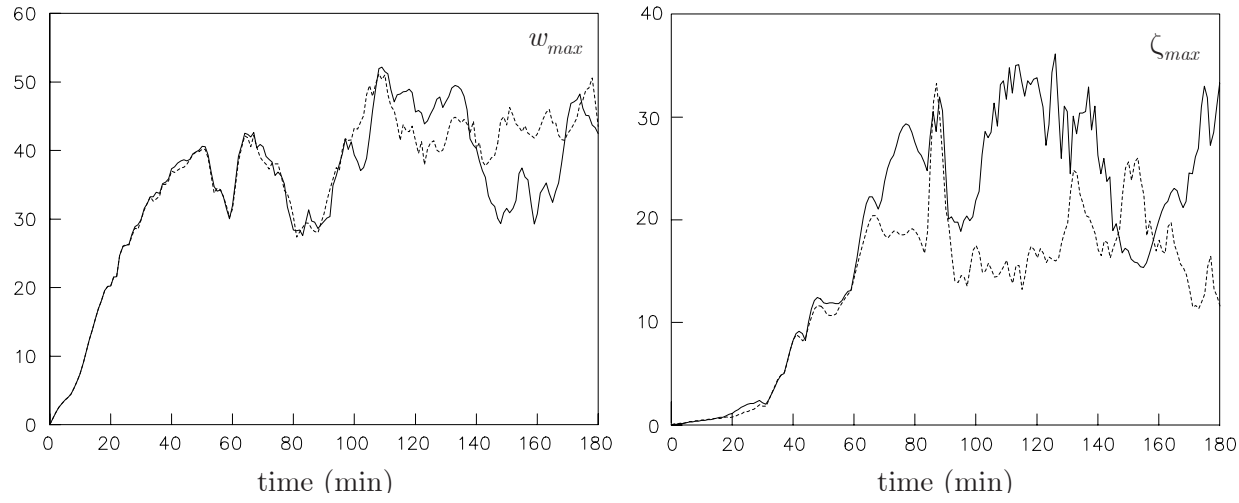

FIG. 4. Time series of maximum vertical velocity, w_{max} (left; m s^{-1}), and maximum vertical vorticity below 2 km, ζ_{max} (right, $\times 10^3$ s^{-1}), in the demonstration simulations without radiative effects (solid) and with emulated anvil radiative effects (dashed).